The Astrophysical Journal Letters, 935:L9 (10pp), 2022 August 10 https://doi.org/10.3847/2041-8213/ac816a

Stars That Approach within One Parsec of the Sun: New and More Accurate Encounters Identified in Gaia Data Release 3

C. A. L. Bailer-Jones
Max Planck Institute for Astronomy, Königstuhl 17, D-69117 Heidelberg, Germany
Received 2022 June 18; revised 2022 July 6; accepted 2022 July 13; published 2022 August 11

Abstract

Close encounters of stars to the Sun could affect life on Earth through gravitational perturbations of comets in the Oort cloud or exposure to ionizing radiation. By integrating orbits through the Galactic potential, I identify which of 33 million stars in Gaia DR3 with complete phase space information come close to the Sun. 61 stars formally approach within 1 pc, although there is high confidence in only 42 (two thirds) of these, the rest being spurious measurements or (in) binary systems. Most of the stars will encounter within the past or future 6 Myr; earlier/later encounters are less common due to the magnitude limit of the Gaia radial velocities (RVs). Several close encountering stars are identified for the first time, and the encounter times, distances, and velocities of previously known close encounters are determined more precisely on account of the significantly improved precision of Gaia DR3 over earlier releases. The K7 dwarf Gl 710 remains the closest known encounter, with an estimated (median) encounter distance of 0.0636 pc (90% confidence interval 0.0595–0.0678 pc) to take place in 1.3 Myr. The new second closest encounter took place 2.8 Myr ago: this was the G3 dwarf HD 7977, now 76 pc away, which approached within less than 0.05 pc of the Sun with a probability of one third. The apparent close encounter of the white dwarf UPM J0812-3529 is probably spurious due to an incorrect RV in Gaia DR3.

Unified Astronomy Thesaurus concepts: Space astrometry (1541); Solar neighborhood (1509)

Supporting material: machine-readable table

1. Introduction

Close encounters between stars can influence the evolution of stellar systems. Early in stars' lives, interactions can disrupt circumstellar disks, potentially influencing planet formation. Later in stars' lives, loosely bound reservoirs of comets, such as the Oort cloud around the Sun, can be perturbed by a close encounter. This can fling comets inward—where they could impact planets—or eject them out of the system, possibly leading to capture by the other star. The close passage of an active star, in particular one that goes supernova, could even jeopardize—or perhaps assist—the evolution of life on a planet.

Of particular interest is the stellar encounter history of the Sun. To identify past or future encounters we need to know stars' current positions and velocities. Extensive searches for encounters were therefore only possible starting with the publication of a hundred thousand parallaxes by Hipparcos in 1997, which increased by orders of magnitude two decades later with Gaia. These data led to the identification of many close encounters (e.g., García-Sánchez et al. 2001; Bobylev & Bajkova 2017; Bailer-Jones et al. 2018b; Wysoczańska et al. 2020b), which fed into modeling how these encounters affected our Oort cloud (e.g., Feng & Bailer-Jones 2015; Torres et al. 2019; Wysoczańska et al. 2020a; Dybczyński & Królikowska 2022).

The present paper continues a study to discover and characterize close encounters, one that started with Hipparcos (Bailer-Jones 2015a; Paper I), then Gaia DR1 (Bailer-Jones 2018; Paper II)—both complemented by non-Gaia data—and most recently Gaia DR2 (Bailer-Jones et al. 2018b; Paper III). Since the first Gaia data release, astrometry has been in abundance and the comparative lack of relative radial velocities (RVs) has been the limiting factor of these studies—a complete reversal of the pre-Hipparcos situation. Gaia DR3 (Gaia Collaboration et al. 2022) now provides radial velocities for 34 million bright stars (99% with $G < 15.7$ mag) with median uncertainties of 3.3 km s^{-1} (central 90% range 0.4–7.8 km s^{-1}). This is nearly a fivefold increase in the number of sources with radial velocities in Gaia DR2, and constitutes the largest radial velocity survey to date.

Here I use these data to identify stars that approach within 1 pc of the Sun. Previous works by various authors have used a larger limit. But as the average spacing[1] between stellar systems in the solar neighborhood (a few tens of parsec) is about 2.2 pc, and the closest stellar neighbor to the Sun—the Alpha Centauri system—is currently just 1.3 pc away, 1 pc seems a more meaningful upper limit. The Oort cloud extends to perhaps 0.25–0.50 pc from the Sun (e.g., Brasser et al. 2012), and even massive stars passing much further from the Sun than this are expected to have only a small effect on the Oort cloud (e.g., Brown & Rein 2022).

2. Data

Gaia DR3 contains 33,653,049 sources with complete six-dimensional phase space coordinates (three positions and three velocities). Of these, 29,947,046 have a parallax signal-to-noise ratio (S/N), `parallax_over_error`, greater than five (prior to adjusting the parallax zero-point). I adopt this as the

[1] By counting the number of stars within some distance we can compute the spacing they would have if they were on a regular cubic lattice. From the Gaia Catalogue of Nearby Stars (Gaia Collaboration et al. 2021) we get values of 2.23–2.33 pc depending on the distance used and whether correcting for incompleteness. Using all sources in Gaia DR3 we get 1.95–2.37 pc for various distances out to 100 pc.

main sample to search for encounters. Less precise parallaxes correspond to less precise encounter parameters, such that even if the median perihelion distance ($d_{\rm ph}^{\rm med}$) were small, its probability distribution would be broad. I nonetheless applied the procedure described in Section 3 to the 3,311,812 sources with $0 < \texttt{parallax\_over\_error} < 5$, but none reached $d_{\rm ph}^{\rm med} < 1$ pc. I did not consider at all the 394,191 sources with $\texttt{parallax\_over\_error} \leqslant 0$. Although it is possible to infer distances for sources with negative parallaxes (e.g., Bailer-Jones 2015b), their distance posteriors are prior-dominated and generally very broad, so the encounter parameters remain very imprecise.

Once selected, I corrected the parallax zero-point of all the sources in the main sample using the procedure described by Lindegren et al. (2021a). This corresponds to increasing the raw parallaxes by 0.006–0.058 mas (central 98% range), the exact value depending on magnitude (as well as color and sky position). Other analyses have suggested that the parallaxes may have to be increased further for the brighter stars in Gaia, by up to 0.015 mas (e.g., Ren et al. 2021; Zinn 2021). This would have little impact on my encounter results, however. Although the raw parallaxes of the main sample cover a broad range, 0.12–7.9 mas (central 98% range), a star will generally have to be closer than about 1 kpc in order to have a high probability of approaching within 1 pc of the Sun, such that any residual error in the parallax zero-point is small compared to the parallax.

There is some evidence that some of the parallax uncertainties in Gaia DR3 are underestimated (e.g., Maíz Apellániz 2022), but I have not inflated them in this study.

An observed radial velocity is often not equal to the true radial velocity for a number of physical reasons beyond measurement or calibration errors. The gravitational redshift increases the observed radial velocity by about 0.6 km s^{-1} for main-sequence stars (less for giants), although this is offset by convective blueshifts that reduce the radial velocity by a similar size. As discussed by Gullberg & Lindegren (2002), the net effect is that the observed minus true radial velocity ranges from about -0.4 km s^{-1} for F stars to $+0.4$ km s^{-1} for K dwarfs. These offsets are generally less than the Gaia DR3 radial velocity uncertainties, and as the specific correction depends on properties that are not well determined for most stars, no correction has been made.

3. Method

Once we have the phase space coordinates and specify the Galactic gravitational potential, the orbits of stars relative to the Sun can be computed by numerical integration. From this we can determine the time, distance, and velocity of closest approach. An accurate numerical integration for all 30 million stars is not only time-consuming, it is also unnecessary, because the vast majority of the stars will never come anywhere near the Sun. Moreover, the uncertainties in (and covariances between) the phase space coordinates must be taken into account. I therefore adopt the following procedure for each star, which is an improvement over the procedure used in Papers I–III (but the method of integration is unchanged).

1. Resample the phase space coordinates 50 times assuming the mean and covariances from Gaia DR3 represent a six-dimensional Gaussian probability distribution over the coordinates, to give 50 "surrogate" stars.
2. Find the closest approach between each surrogate and the Sun under the assumption of nonaccelerated motion, i.e., neglecting gravity. This linear motion approximation (LMA) has a simple analytic solution (Section 3.2 of Paper I).
3. If any of the 50 surrogates from the previous step approach within $d_{\rm lim} = 7.07$ pc of the Sun, numerically integrate the orbits of all 50 surrogates through the Galactic potential. This uses 50 time steps distributed uniformly over the interval $[0, 2t_{\rm ph}^{\rm LMA}]$, where $t_{\rm ph}^{\rm LMA}$ is the time of closest approach computed from the LMA (for that surrogate).
4. If any of the 50 surrogates from the previous step approach within $d_{\rm lim} = 7.07$ pc of the Sun, do a higher resolution numerical integration using 1000 surrogates each integrated for 500 time steps.
5. Determine whether the median (over the 1000 surrogates; $d_{\rm ph}^{\rm med}$) encounter distance is below 1 pc.

Only the stars that make it through the final step are reported here. Using the distributions over the perihelion time ($t_{\rm ph}$, signed), distance ($d_{\rm ph}$, nonnegative), and velocity ($v_{\rm ph}$, nonnegative), I compute their medians as well as their 5% and 95% quantiles, the latter two providing the 90% central confidence interval (CI) for each parameter.

$d_{\rm lim}$ was chosen to be large enough to make it likely that the selections in steps three and four include all encounters that will come within 1 pc when integrated at high resolution in step five. If $d_{\rm lim}$ is lowered to 5 pc then in fact we miss two encounters.[2] It is therefore possible that a few more encounters would be found if we used a larger $d_{\rm lim}$, although this gets increasingly unlikely.

The LMA in step two is reasonably accurate in many cases, and good enough for the first liberal selection, because many stars travel only a short distance from their current location to perihelion, so their paths are relatively unaccelerated by the Galactic potential. The gravitational potential used in steps three and four is a simple, three-component axisymmetric model described in Section 3.3 of Paper I. Because the accelerations are not large, the results are not very sensitive to the exact potential or location of the Sun in the Galaxy. As discussed in Section 5.2 of Paper I, close encounters of a star on its journey to perihelion with other individual stars will hardly affect its orbit in the vast majority of cases. We may, therefore, reasonably adopt a smooth potential.

Light travel times have been neglected in the computations. This makes the inferred encounter times too late (too positive) by an amount roughly equal to the light travel time, which in the worst case is about 1 kyr. The fractional error this introduces in the encounter time is approximately the ratio of the radial velocity to the speed of light, which is of order 4×10^{-4}. As we will see, this is much smaller than the uncertainties arising from the Gaia measurements.

For a very close encountering star, or one with large measurement uncertainties, it is possible that the orbits of the surrogates—which represent these uncertainties—pass the Sun on opposite sides. If we then calculated the average of the *signed Cartesian coordinates* of these surrogates at perihelion, this average could be arbitrarily close to zero, on account of the canceling of positive and negative coordinates (surrogates

[2] $(7.07/5)^2 \simeq 2$. The expected number of encounters within a distance d scales as d^2 (Bailer-Jones 2018).

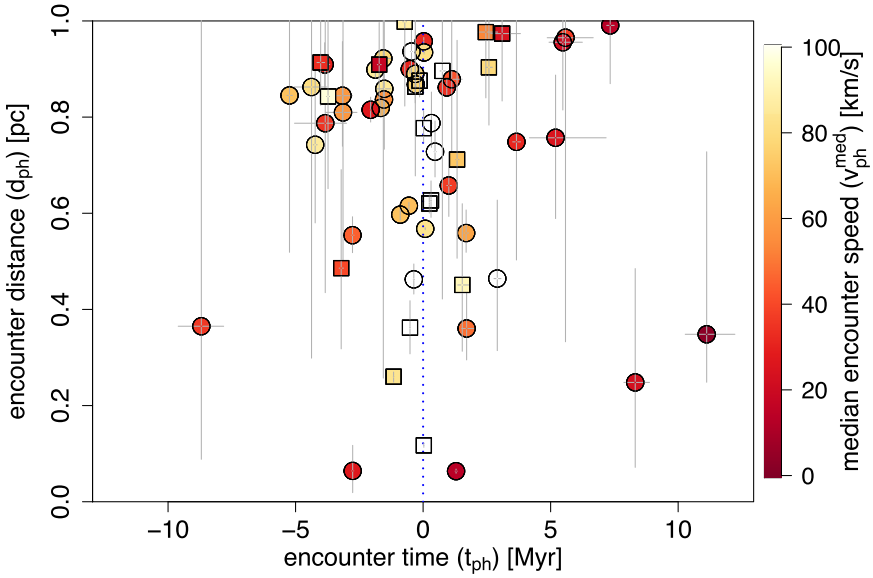

Figure 1. Perihelion (encounter) times and distances for the 61 stars that have a median perihelion distance ($d_{\rm ph}^{\rm med}$) below 1 pc. Negative times indicate past encounters, positive times future ones. The circles/squares show the median of the perihelion time and distance distributions computed from the 1000 data resamples (surrogates); the error bars show the 5th and 95th percentiles. Circles denote good encounters; squares denote the questionable encounters, which are marked with a † or b in Table 1. The color of each point indicates the median encounter velocity; those faster than 100 km s^{-1} are white.

passing on either side). But this is clearly not a useful measure of the average perihelion *distance*. We must instead look at the distribution of the (nonnegative) perihelia distances over the surrogates, and then average those. This is what I do in this work (and did in Papers I–III), using the quantiles of the distribution to characterize the distribution. Not all studies do this (e.g., Dybczyński et al. 2022), and the average signed coordinate will always produce a lower "distance" than the average of the nonnegative distances. In principle a similar problem can also occur with the encounter time or velocity if the radial velocity is near zero. The encounter times I compute are signed, but we can see from the distribution (see Paper I) — summarized by the 90% CI—whether some times have a different sign. This does not occur for any of the encounters in this study.

4. Results

4.1. Overall Results

Of the 29,947,046 stars subject to the LMA analysis in step two of the procedure in Section 3, 11,199 had at least one surrogate with $d_{\rm ph} < 7.07$ pc and so were processed in step three. Of those, 6407 had at least one surrogate with $d_{\rm ph} < 7.07$ pc in the low resolution orbit integration and so were processed in step four. Of those, 1892 had a median encounter distance ($d_{\rm ph}^{\rm med}$) below 5 pc following the high resolution orbital integration and 61 have $d_{\rm ph}^{\rm med} < 1$ pc; this is the sample that I examine in the rest of this paper.

Figure 1 shows the encounter times, distances, and velocities of the 61 closest encounters. Most of the encounters take place within 6 Myr of the present date. Larger absolute times correspond to stars that are currently further away and/or that have low velocities relative to the Sun. This "time horizon" of the encountering stars arises from them having a characteristic maximum distance due to the magnitude limit of the main sample. This, combined with a characteristic velocity relative to the Sun, means most stars cannot travel for more than a few million years to/from their encounter and be visible now.

Table 1 lists the encounter parameters as well as the parallaxes, proper motions, and radial velocities of the 61 closest encounters. The final column of the table gives the ratio of the current absolute radial velocity (v_r) to the current transverse velocity (v_t) of each star. The fact that these ratios are generally much larger than one is a selection effect: stars that approach close to the Sun are those that are currently moving almost directly toward or away from it, so have $|v_r| \gg v_t$. It is therefore not surprising that many of the close encounters have large absolute radial velocities. Nonetheless, we see several encounters with radial velocities (and thus space velocities) above several hundred kilometers per second. While such velocities do occur, we should be suspicious of these, as they could be a result of an incorrect template or failure of the cross-correlation in the Gaia processing reported in Katz et al. (2022). This will be discussed for some individual cases in Section 4.2.

Table 2 provides additional information on the encounters. M_G is the absolute magnitude of the source on the assumption of zero extinction and $1/\varpi$ being a reasonable distance estimate, which it is because the parallax S/N is above 30 for all but three of the sources (and those still have S/Ns above 10); `ruwe` is a calibrated reduced χ^2 of the astrometric solution. Values much more than a few could indicate the astrometric solution is poor, although this is not a definitive metric; `astrometric_params_solved` is 31 if the astrometric solution was for the standard five parameters (two positions, parallax, two proper motions), and 95 if the color of the source was solved in addition, for reasons discussed in Lindegren et al. (2021b); `ipd_frac_multi_peak` indicates the percentage of image windows used in the astrometry, which contain more than one peak. This may indicate it is a double star (physical or otherwise), although only two of the stars in the table have a definite indication of physical close binarity in Gaia DR3 (rows 13 and 58); `rv_expected_sig_to_noise` is the estimated S/N of the spectrum used to determine

Table 1
Perihelion (encounter) Parameters For all Stars With a Median Perihelion Distance ($d_{\rm ph}^{\rm med}$) Below 1 pc, Sorted by Increasing $d_{\rm ph}^{\rm med}$

		1	2	3	4	5	6	7	8	9	10	11	12	13	14	15	16	17
		Gaia DR3 source_id	$t_{\rm ph}$ [kyr]			$d_{\rm ph}$ [pc]			$v_{\rm ph}$ [km s^{-1}]			ϖ	$\sigma(\varpi)$	μ	$\sigma(\mu)$	v_r	$\sigma(v_r)$	$\lvert v_r/v_t\rvert$
			med	5%	95%	med	5%	95%	med	5%	95%	mas		mas yr^{-1}		km s^{-1}		
	1	4270814637616488064	1292	1257	1334	0.064	0.060	0.068	14.4	14.0	14.8	52.43	0.02	0.43	0.02	−14.4	0.3	373
	2	510911618569239040	−2761	−2798	−2720	0.064	0.019	0.117	26.8	26.4	27.2	13.24	0.03	0.14	0.02	26.8	0.2	517
†	3	5544743925212648320	29	28	30	0.117	0.113	0.122	374.3	359.7	387.1	89.54	0.02	71.70	0.02	−373.7	8.2	98
	4	213090546082530816	8316	7874	8874	0.248	0.072	0.485	23.0	21.5	24.3	5.07	0.01	0.45	0.01	−23.5	0.8	56
b	5	5571232118090082816	−1157	−1166	−1146	0.260	0.249	0.270	82.6	81.9	83.3	10.24	0.01	0.47	0.01	82.5	0.4	379
	6	5469802896279029504	11119	10281	12222	0.348	0.249	0.728	3.2	2.9	3.4	29.40	0.02	2.39	0.02	−2.7	0.2	7
	7	3372104035275483392	1706	1518	1982	0.360	0.295	0.441	47.6	41.0	53.5	12.03	0.04	0.71	0.04	−47.4	3.7	170
†	8	3207963476278403200	−514	−529	−498	0.362	0.308	0.418	515.1	506.1	525.5	3.69	0.05	0.81	0.04	515.5	5.8	496
	9	3106500096597409792	−8695	−9599	−7823	0.365	0.088	1.027	36.2	32.7	40.1	3.09	0.01	0.48	0.01	36.9	2.2	50
b	10	4763293626627587840	1535	1361	1788	0.451	0.313	0.620	92.0	78.7	103.6	6.93	0.05	0.39	0.06	−91.1	7.4	341
	11	929788371508812288	−364	−384	−343	0.463	0.432	0.494	195.3	184.9	207.0	13.76	0.06	3.82	0.05	195.7	6.6	149
	12	6913732624445112832	2908	2782	3051	0.464	0.314	0.627	105.2	100.1	109.6	3.21	0.02	0.73	0.02	−104.1	2.9	96
†	13	3118526069444386944	−3212	−3293	−3125	0.486	0.318	0.691	40.0	39.1	40.9	7.61	0.05	0.26	0.05	40.1	0.5	251
	14	6608946489396474752	−2768	−2819	−2712	0.554	0.518	0.593	44.8	44.0	45.7	7.95	0.01	0.72	0.01	43.8	0.5	102
	15	3295253979286613376	1687	1610	1782	0.559	0.519	0.607	61.8	58.4	64.7	9.38	0.02	0.67	0.02	−61.6	1.9	181
	16	1952802469918554368	83	82	83	0.568	0.566	0.570	83.2	82.9	83.5	141.94	0.02	201.01	0.02	−82.9	0.2	12
	17	5261593808165974784	−896	−907	−883	0.597	0.586	0.608	71.1	70.2	72.1	15.35	0.01	2.21	0.01	71.1	0.6	104
	18	3054509410098672000	−557	−561	−552	0.616	0.609	0.622	70.3	69.8	71.0	24.97	0.02	5.53	0.02	70.4	0.4	67
†	19	3001468183198140800	242	238	246	0.620	0.601	0.638	885.7	873.0	896.8	4.56	0.03	1.66	0.03	−885.2	7.1	513
†	20	4116451378388951424	311	294	329	0.627	0.592	0.667	264.8	254.9	273.4	11.91	0.33	4.22	0.17	−264.4	5.5	158
	21	3600338081985998080	1008	930	1109	0.658	0.594	0.727	37.4	34.0	40.4	25.97	0.08	3.19	0.11	−37.2	1.9	64
†	22	4536673181955253504	1332	1278	1396	0.712	0.507	0.960	71.8	70.3	73.1	10.24	0.25	1.04	0.22	−71.7	0.9	149
	23	398469656625177216	467	432	515	0.728	0.676	0.792	151.9	137.8	164.3	13.78	0.04	4.15	0.04	−151.4	7.9	106
	24	3007538204640292480	−4232	−4302	−4157	0.742	0.580	0.919	86.4	85.2	87.7	2.67	0.01	0.44	0.01	86.5	0.8	110
	25	911145876981562496	3660	3514	3818	0.749	0.503	1.014	31.2	29.9	32.3	8.61	0.09	0.82	0.09	−30.7	0.7	68
	26	2184252351930210560	5194	4172	7173	0.757	0.589	0.887	24.7	17.9	30.7	7.65	0.02	0.59	0.02	−24.1	3.9	66
†	27	3320184202856435840	19	18	20	0.777	0.748	0.813	416.6	398.1	432.8	123.24	0.02	1026.46	0.01	−414.0	10.4	10
	28	6483100752169539584	−3837	−5038	−3006	0.787	0.435	1.066	34.9	26.8	44.3	7.35	0.04	1.49	0.04	34.4	5.4	36
	29	4155835025908320640	327	308	349	0.788	0.737	0.852	283.7	264.6	300.4	10.55	0.04	5.89	0.04	−283.0	10.7	107
	30	3443909634992792320	−3140	−3814	−2596	0.810	0.486	1.216	58.0	47.7	69.8	5.36	0.09	0.29	0.08	58.7	6.6	230
	31	6726602067616477056	−2057	−2074	−2038	0.815	0.790	0.841	26.8	26.6	27.1	17.70	0.03	1.79	0.03	26.9	0.1	56
	32	2926732831673735168	−1658	−1665	−1650	0.819	0.803	0.835	66.5	66.3	66.8	8.87	0.01	0.91	0.01	66.5	0.2	137
	33	1791617849154434688	−1533	−1545	−1520	0.837	0.819	0.854	55.9	55.5	56.3	11.42	0.02	1.23	0.01	55.8	0.3	109
b	34	3101404272522355584	−3728	−3781	−3672	0.843	0.651	1.043	97.2	96.5	98.0	2.70	0.02	0.23	0.02	97.4	0.4	242
	35	3218956015577464064	−3162	−3595	−2769	0.845	0.740	0.957	58.1	51.1	66.1	5.33	0.03	0.63	0.02	58.4	4.5	104
	36	2929487348824926336	−5238	−5338	−5128	0.845	0.519	1.167	70.8	69.9	71.8	2.64	0.02	0.45	0.02	70.7	0.6	88
	37	3621143693841328896	−1522	−1823	−1276	0.859	0.733	1.047	85.0	71.0	101.0	7.57	0.05	0.87	0.06	85.2	9.0	156
	38	3260079227925564160	929	912	947	0.862	0.846	0.878	32.8	32.1	33.3	32.13	0.03	6.14	0.03	−32.7	0.4	36
†	39	3222258501830719616	−4375	−5066	−3774	0.863	0.299	1.531	80.0	69.3	92.2	2.80	0.05	0.73	0.04	80.4	6.9	65
†	40	775766686745320960	−305	−351	−269	0.863	0.678	1.131	394.3	382.9	407.3	8.14	0.59	4.09	0.49	394.7	7.3	166
	41	5346007675222666752	−285	−287	−282	0.868	0.859	0.875	76.3	75.7	77.1	44.99	0.02	28.02	0.02	76.3	0.4	26
†b	42	5473864079915092736	−137	−142	−132	0.876	0.842	0.909	711.6	689.6	736.7	10.04	0.05	12.92	0.05	712.5	14.1	117
	43	899893234465049216	1122	908	1529	0.879	0.709	1.194	41.5	30.4	51.3	20.99	0.04	3.80	0.03	−41.1	6.2	48
	44	5553958176239495040	−309	−330	−288	0.890	0.830	0.949	78.5	73.5	84.1	40.32	0.02	24.00	0.03	78.6	3.2	28
†	45	4041250662947214464	755	667	868	0.896	0.422	1.452	162.7	150.8	173.2	7.99	0.57	2.09	0.72	−162.3	6.7	131

Table 1
(Continued)

		1	2	3	4	5	6	7	8	9	10	11	12	13	14	15	16	17
		Gaia DR3 source_id	t_{ph} [kyr]			d_{ph} [pc]			v_{ph} [km s^{-1}]			ϖ	$\sigma(\varpi)$	μ	$\sigma(\mu)$	v_r	$\sigma(v_r)$	$\lvert v_r/v_t \rvert$
			med	5%	95%	med	5%	95%	med	5%	95%	mas		mas yr^{-1}		km s^{-1}		
	46	2924378502398307840	−1871	−1889	−1851	0.899	0.880	0.919	85.6	84.8	86.4	6.11	0.01	0.76	0.01	85.5	0.5	145
	47	3972130276695660288	−522	−526	−517	0.900	0.891	0.908	31.2	30.9	31.5	59.96	0.03	21.84	0.03	31.1	0.2	18
b	48	1132123559268892288	2581	2473	2712	0.904	0.784	1.033	78.0	74.2	81.3	4.87	0.01	0.38	0.02	−77.3	2.1	210
b	49	6224087389269263488	−1722	−1793	−1647	0.909	0.830	0.996	18.0	17.3	18.8	31.47	0.15	3.28	0.17	18.0	0.4	36
	50	5551538941421122304	−3858	−4048	−3661	0.910	0.860	0.955	30.1	28.7	31.7	8.46	0.01	1.04	0.01	29.7	0.9	51
b	51	2933503521200215424	−4017	−4160	−3860	0.914	0.825	1.022	32.7	31.5	34.0	7.46	0.02	0.25	0.01	32.7	0.7	206
	52	2020810807491120896	−1560	−1936	−1270	0.922	0.257	2.050	76.8	68.8	85.8	8.19	0.82	0.84	0.66	77.0	5.1	159
	53	1926461164913660160	36	36	37	0.934	0.931	0.938	80.9	80.6	81.2	316.54	0.04	1595.62	0.03	−77.3	0.2	3
	54	3142271161216457472	−455	−496	−415	0.936	0.850	1.025	114.0	104.5	124.9	18.83	0.05	8.52	0.06	114.4	6.1	53
	55	5896469620419457536	5479	4940	6241	0.956	0.815	1.047	20.6	18.0	22.8	8.68	0.02	0.78	0.01	−20.5	1.4	48
	56	5853498713190525696	27	27	27	0.958	0.951	0.965	32.4	32.1	32.6	768.09	0.05	3859.23	0.03	−21.9	0.2	1
	57	1726458694148645888	5583	4869	6666	0.965	0.333	2.667	37.5	31.5	42.8	4.73	0.02	1.14	0.02	−35.9	3.5	31
†	58	418338821185634048	3098	2654	3813	0.974	0.834	1.172	24.2	19.6	28.3	13.04	0.04	0.94	0.04	−24.0	2.6	70
b	59	6899603831309106560	2460	2156	2921	0.977	0.840	1.181	53.0	44.6	60.4	7.51	0.03	0.92	0.02	−52.4	4.7	90
	60	3676827188919831936	7335	7202	7490	0.991	0.870	1.105	13.9	13.6	14.1	10.10	0.02	1.63	0.02	−11.8	0.2	15
†	61	5614610776700908672	−718	−793	−654	0.998	0.823	1.206	88.4	81.9	95.8	15.38	0.49	4.50	0.30	88.7	4.2	64

Note. Columns 2, 5, and 8 are t_{ph}^{med}, d_{ph}^{med}, and v_{ph}^{med} respectively. The columns labeled 5% and 95% are the bounds of the corresponding confidence intervals. Columns 11–16 list the current parallax (ϖ, including the zero-point offset), total proper motion (μ), and radial velocity (v_r), along with their 1-sigma uncertainties. Column 17 is the ratio of the current absolute radial velocity to the current transverse velocity, the latter computed as 4.74047 μ/ϖ. On the far left, † indicates that the encounter is dubious for a variety of possible reasons, and b indicates it is probably in a wide binary system according to El-Badry et al. (2021), so may also not be reliable. A machine readable version of Tables 1 and 2 (combined into a single table) reporting values to more significant figures is available in the online Journal and at this URL.

(This table is available in its entirety in machine-readable form.)

Table 2
Additional Data on the Close Encounters Listed in Table 1

	Gaia DR3 source_id	G (mag)	BP − RP (mag)	M_G (mag)	ruwe	astrometric_ params_solved	ipd_frac_ multi_peak	rv_expected_ sig_to_noise	rv_nb_ transits	l (deg)	b (deg)
1	4270814637616488064	9.06	1.69	7.66	0.91	31	0	132.6	6	28	6
2	510911618569239040	8.89	0.76	4.50	2.01	31	0	188.8	18	126	−1
3	5544743925212648320	14.35	0.68	14.11	1.04	31	0	6.2	16	253	−1
4	213090546082530816	12.06	0.99	5.58	1.05	31	0	38.8	25	161	5
5	5571232118090082816	11.78	1.49	6.83	0.93	31	26	31.2	9	250	−25
6	5469802896279029504	10.08	1.62	7.42	1.30	31	0	119.3	13	271	29
7	3372104035275483392	15.31	2.57	10.70	0.97	31	0	3.7	8	194	4
8	3207963476278403200	14.89	2.63	7.69	1.08	95	28	4.2	9	208	−25
9	3106500096597409792	12.79	0.89	5.22	0.99	31	0	15.9	11	214	−3
10	4763293626627587840	16.00	2.75	10.19	1.24	95	14	3.4	17	266	−34
11	929788371508812288	15.83	3.20	11.52	1.10	31	2	2.3	6	173	32
12	6913732624445112832	14.53	1.38	7.04	1.01	31	0	7.8	33	43	−30
13	3118526069444386944	12.14	1.61	6.55	3.19	31	0	30.5	12	210	−7
14	6608946489396474752	12.27	1.42	6.76	1.07	31	0	31.5	15	24	−61
15	3295253979286613376	14.33	2.35	9.18	1.09	31	0	15.3	28	188	−19
16	1952802469918554368	10.83	2.81	11.59	1.19	31	8	145.0	25	88	−12
17	5261593808165974784	12.68	2.02	8.61	1.14	31	0	38.7	25	286	−27
18	3054509410098672000	12.40	2.56	9.39	1.43	31	1	51.5	21	224	6
19	3001468183198140800	15.24	2.08	8.51	1.07	31	0	4.2	7	219	−12
20	4116451378388951424	15.80	1.90	11.17	3.58	95	74	2.2	6	4	4
21	3600338081985998080	14.19	2.81	11.26	3.24	31	0	18.1	23	275	56
22	4536673181955253504	13.47	2.32	8.51	20.37	31	0	27.6	32	53	16
23	398496965625177216	15.45	2.85	11.14	1.06	31	0	3.3	2	128	−15
24	3007538204640292480	12.36	0.82	4.48	1.09	31	0	24.1	16	216	−10
25	911145876981562496	12.48	1.50	7.15	6.28	31	0	32.1	16	184	35
26	2184252351930210560	15.16	2.47	9.56	1.07	31	0	6.9	21	87	9
27	3320184202856435840	13.97	0.83	14.42	0.92	95	0	6.5	12	202	−10
28	6483100752169539584	15.52	2.45	9.84	1.04	31	0	3.9	19	353	−42
29	4155835025908320640	15.26	2.75	10.37	0.97	31	0	2.9	4	22	1
30	3443909634992792320	14.04	1.69	7.67	2.58	95	99	6.8	4	180	2
31	6726602067616477056	9.18	0.98	5.42	1.23	31	17	54.7	2	354	−12
32	2926732831673735168	9.56	0.71	4.30	1.02	31	0	148.2	22	231	−12
33	1791617849154434688	11.00	1.08	6.28	1.01	31	0	80.5	23	71	−18
34	3101404272522355584	11.22	0.67	3.34	1.12	31	0	31.3	9	219	−0
35	3218956015577464064	14.85	2.02	8.47	1.00	31	0	6.7	24	206	−16
36	2929487348824926336	11.22	0.77	3.30	1.30	95	0	47.5	17	233	−5
37	3621143693841328896	15.55	2.29	9.93	1.16	31	0	3.6	11	310	49
38	3260079227925564160	11.73	2.13	9.27	1.62	31	0	64.1	16	189	−34
39	3222258501830719616	15.16	2.51	7.35	1.79	31	0	8.4	20	201	−18
40	775766686745320960	15.91	2.91	10.45	13.85	31	15	3.6	8	183	62
41	5346007675222666752	12.46	2.69	10.72	1.19	31	0	53.3	23	290	5
42	5473864079915092736	15.64	2.93	10.64	1.42	31	0	4.0	12	263	27
43	899893234465049216	14.96	2.72	11.56	1.15	31	0	4.3	4	180	22
44	5553958176239495040	14.79	3.29	12.82	1.23	31	0	10.6	24	255	−24
45	4041250662947214464	16.26	2.54	10.76	12.32	95	52	5.1	13	354	−3
46	2924378502398307840	12.61	1.23	6.53	0.99	31	0	39.2	38	232	−16
47	3972130276695660288	9.88	2.17	8.77	1.18	31	0	143.4	12	228	66

Table 2
(Continued)

	Gaia DR3 source_id	G (mag)	BP − RP (mag)	M_G (mag)	ruwe	astrometric_ params_solved	ipd_frac_ multi_peak	rv_expected_ sig_to_noise	rv_nb_ transits	l (deg)	b (deg)
48	1132123559268892288	13.64	1.41	7.06	0.95	31	0	11.4	18	133	34
49	6224087389269263488	10.64	1.85	8.13	8.44	31	32	59.7	6	334	26
50	5551538941421122304	13.08	1.70	7.71	1.02	31	0	26.4	19	258	−22
51	2933503521200215424	8.79	0.51	3.14	0.89	31	1	189.1	19	230	−9
52	2020810807491120896	14.79	1.96	9.34	8.07	95	30	9.2	33	61	1
53	1926461164913660160	10.38	3.53	12.88	1.03	31	8	142.5	12	110	−17
54	3142271161216457472	15.75	3.13	12.12	1.14	31	0	3.7	11	211	13
55	5896469620419457536	13.53	1.98	8.21	0.97	31	1	17.0	24	314	7
56	5853498713190525696	8.98	3.80	13.41	0.97	95	11	222.3	7	314	−2
57	1726458694148645888	14.65	1.95	8.01	1.03	31	0	8.2	23	124	32
58	418338821185634048	14.76	2.87	10.33	2.12	31	0	11.1	30	122	−8
59	6899603831309106560	14.76	2.15	9.13	1.16	31	0	7.6	18	32	−29
60	3676827188919831936	10.12	0.88	5.14	0.97	31	0	134.2	31	302	57
61	5614610776700908672	14.36	1.05	10.29	29.74	95	27	8.1	41	241	−0

Note. All fields are taken directly from the Gaia DR3 gaia_source table, except for M_G, which is $G + 5\log_{10}(\varpi/100)$, where ϖ is the zero-point-corrected parallax in milliarcseconds. Descriptions of the other fields can be found in the Gaia DR3 online documentation: gea.esac.esa.int/archive/documentation/GDR3/Gaia_archive/chap_datamodel/sec_dm_main_source_catalogue/ssec_dm_gaia_source.html.

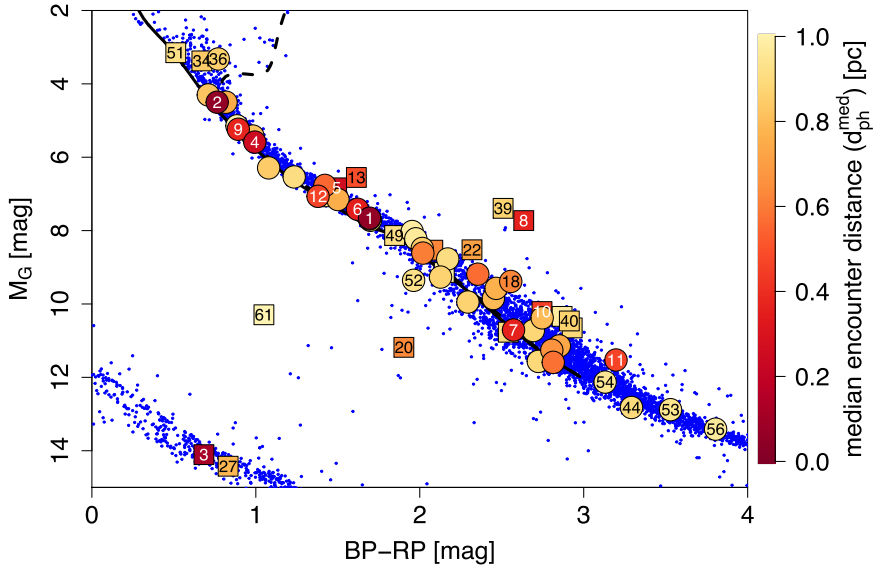

Figure 2. Color–absolute magnitude diagram, with M_G computed assuming zero extinction. The red/yellow colored points are the 61 encounters with $d_{\rm ph}^{\rm med} < 1$ pc identified in this work, color coded according to $d_{\rm ph}^{\rm med}$. Circles denote good encounters; squares denote the questionable encounters, which are marked with a † or b in Table 1. The 13 encounters with $d_{\rm ph}^{\rm med} < 0.5$ pc plus several others of possible interest are labeled by their order of increasing distance (row number in Table 1). For orientation, the black lines are unreddened solar metallicity PARSEC isochrones for 1 Gyr (solid) and 10 Gyr (dashed) from Marigo et al. (2017), and the small blue dots are a random subset of all sources in Gaia DR3 with $\varpi > 50$ mas and `ruwe` < 1.2.

the RV, and `rv_nb_transits` is the number of measurement epochs used in that determination; l and b are the Galactic longitude and latitude of the star.

Figure 2 shows the location of encounters in the color–absolute magnitude diagram. The median distance to these stars is 100 pc (maximum 380 pc), so in most cases the assumption of negligible extinction is valid. The location of the stars in this diagram, as well as the stellar parameters provided in Gaia DR3 for many of them by Andrae et al. (2022), show that most of the stars are main-sequence FGKM stars. In addition there are two white dwarfs, two possible very young stars lying above the main sequence, and two stars lying unexpectedly between the white dwarf and main sequences. These will be discussed in the next section.

Encounters that are dubious are prefixed with a † in Table 1. This assignment occurs because the RV is suspiciously large, the `ruwe` is large, or for another reason given in the next section. Eight stars that are probably in wide binaries according to the criteria of El-Badry et al. (2021) are prefixed with a "b." Unless the orbital period is very long compared to the time to encounter ($t_{\rm ph}^{\rm med}$), the orbital motion will be significant, and hence the Galactic trajectory computed in the present work will be incorrect. El-Badry et al. (2021) does not list periods, only projected separations (which range from 10^2 to 10^4 au for these eight stars), so until a long period can be confirmed for any of these stars, their solar encounters should be regarded as unreliable. Two other stars in Table 1 (6608946489396474752 and 3001468183198140800) are also listed in this wide binary catalog, but they are probably chance alignments (values of `R_chance_align` of 0.44 and 2.3, respectively, whereas the ones denoted "b" have 0.07 or—generally—much less).

4.2. Specific Close Encounters

Here I discuss selected sources from Table 1 giving the row number, Gaia `source_id`, and the primary Simbad name for the source, if available. The `source_id` has not changed from EDR3 to DR3 (other than this prefix).

1: Gaia DR3 4270814637616488064 = Gl 710. Since Hipparcos, this K7 dwarf has often held the title of the closest known bona fide encounter. In Paper I (Hipparcos) it had a median encounter distance of 0.267 pc with a 90% CI of 0.101–0.444 pc. In Paper III (Gaia DR2) this was significantly reduced to 0.0676 pc (90% CI 0.0519–0.0842 pc) where it was the closest encounter found. This does not change much using Gaia DR3—the median is 0.0636 pc—but it is more precise with a 90% CI of 0.0595–0.0678 pc. This is mostly due to a factor of three improvement in the precision of both its parallax and proper motions. Assuming Gl 710 has a mass of 0.7 $M_\odot$ (Paper III) the gravitational attraction by the Sun only lowers the median perihelion by 7 au (35 μpc, 0.06%) demonstrating that gravitational focusing can be neglected in all these encounters.

2: Gaia DR3 5109116185692390 40 = HD 7977. This G3 dwarf was found in Gaia DR2 (Paper III) as a close encounter with a median distance of 0.429 pc (90% CI 0.368–0.494 pc), but now comes much closer with a median of 0.0641 pc (90% CI 0.0191–0.1171 pc). This is mostly due to a significant reduction in its proper motion. There is a large relative uncertainty in the encounter distance because the S/N of the proper motion is low, just 4.2. Yet this is the only known star with a significant probability—32%—of approaching within 0.05 pc of the Sun. The `ruwe` is slightly inflated (2.01), which could suggest a problem with the astrometric solution, although there is no indication of close binarity. Dybczyński et al. (2022) found a much closer minimum perihelion distance for this star using Gaia EDR3 (which has the same astrometry as DR3, but different RVs), but this is partly because they averaged the *signed* coordinates of the surrogates (Section 3), which underestimates the distance in this case (see their Figure 5).

3: Gaia DR3 5544743925212648320 = UPM J0812-3529. This was discovered to be a nearby white dwarf by Finch et al. (2018), but Gaia DR3 is the first publication of a radial velocity. If a real encounter, then it will pass just 0.11 pc from the Sun in 29 kyr. However, the radial velocity is suspiciously large ($-374\,\mathrm{km\,s^{-1}}$), even though the ratio to the transverse velocity is modest (it has a large proper motion and is currently just 11.2 pc away). It is hard to measure radial velocities for white dwarfs accurately on account of their relatively featureless spectra, especially in this case due to its apparently strong magnetic fields (Bagnulo & Landstreet 2020). The Gaia DR3 RV pipeline does not include any white dwarf templates, and although the main-sequence dwarf template $T_{\rm eff}$ of 6000 K is close to the value of 6090 K estimated by Bagnulo & Landstreet (2020), the Gaia DR3 RV is likely wrong (Gaia CU6 (RV) team, private communication). If it is correct, the strong gravitational redshift in white dwarfs means that the true RV of the star would be tens of kilometers per second more negative. As the RV of this star is negative, the true absolute value of its RV would be even larger and the encounter even closer. If the gravitational redshift were $30\,\mathrm{km\,s^{-1}}$, for example, the star would come about 0.008 pc (7%) closer.

4: Gaia DR3 213090546082530816 = UCAC4 689-035468. This was found in Paper III but with a much larger median encounter distance of 1.44 pc and large uncertainty (90% CI) of 0.703–2.175 pc. These have now decreased to 0.248 pc and 0.072–0.489 pc, respectively, thanks to more precise astrometry.

6: Gaia DR3 5469802896279029504 = CD-25 8217. At 11 ± 1 Myr; this is the latest encounter. It is also the slowest encounter, moving at just $3.2\,\mathrm{km\,s^{-1}}$ relative to the Sun. Both of these are a consequence of its small radial velocity of $-2.66 \pm 0.17\,\mathrm{km\,s^{-1}}$. RAVE DR6 (Steinmetz et al. 2020) reports an RV of $-4.02 \pm 1.06\,\mathrm{km\,s^{-1}}$. If we use this in the orbital integration we get a larger median perihelion distance of 0.92 pc with a wider 90% CI of 0.32–1.10 pc, and an encounter that probably takes places sooner, at 7.7 Myr, but with a larger spread due to the larger RV uncertainty (90% CI 5.6–12.9 Myr).

8: Gaia DR3 3207963476278403200. This has a suspiciously high RV of $515 \pm 6\,\mathrm{km\,s^{-1}}$. There is a second source in Gaia DR3 1.″0 away that is 1.1 mag fainter; this could have interfered with the radial velocity determination. The RV spectrum also has a very slow S/N. The star also lies well above the main sequence (Figure 2). This can indicate binarity, although a three magnitudes offset is far too large. It could instead be a pre-main-sequence star (see object 39 below), in which case the RV is likely wrong due to a lack of appropriate templates in the data processing.

13: Gaia DR3 3118526069444386944. This was identified as a young stellar object candidate by Zari et al. (2018). It was found in Paper III to encounter at 1.03 pc; now apparently reduced to 0.49 pc. However, it is just one of two stars in Table 1 that is identified as a close physical binary in Gaia DR3 via the `non_single_star` flag (the other is object 58). Specifically, it is an astrometric binary with a significant proper motion acceleration (a so-called seven-parameter solution). The table `nss_acceleration_astro` lists improved parallaxes and proper motions that take into account this acceleration, but as they still may not be representative of the center of mass of the binary system, I have not recomputed the encounter. This encounter should be disregarded until the system motion has been adequately characterized.

20: Gaia DR3 4116451378388951424. This star is strange because it lies in the otherwise relatively empty region between the white dwarf and main sequences. After Gaia DR2 it was found that many stars in this region were very faint ($G \gtrsim 19.5$ mag) and had spuriously large parallaxes. This situation has greatly improved in Gaia DR3, but as this star has a large `ruwe`, its astrometric solution may well be inappropriate. It lies very close to the Galactic center in a crowded field, so it is possible that a nearby star has affected the measurement. This should lead us to doubt the surprisingly large RV too (which is extracted from a very low S/N spectrum).

27: Gaia DR3 3320184202856435840 = EGGR 290. The apparent close encounter of this white dwarf in just 19 kyr is likely erroneous on account of its unreliable large RV (see object three above).

39: Gaia DR3 3222258501830719616 = CVSO 29. This is a T Tauri star in the Orion OB1 association. The fact that it is still contracting toward the main sequence explains its position above the main sequence in Figure 2, although any circumstellar dust extinction and reddening has not been taken into account in that plot. This encounter supposedly occurred 4.4 Myr ago, but the star had probably not even formed at that time. It is quite likely that interactions in its birth cluster have modified its motion. This encounter must be disregarded.

53: Gaia DR3 1926461164913660160 = Ross 248. This is currently one of the closest stars to the Sun at 3.2 pc. It will come closer in 36 kyr, to 0.934 pc; 7 kyr before this it will pass within 0.46 pc of the interstellar object 'Oumuamua (Bailer-Jones et al. 2018a).

56: Gaia DR3 5853498713190525696 = Proxima Cen. It appears that our closest neighbor will get slightly closer in 27 kyr, although its orbit around Alpha Centauri AB needs to be taken into account. This was done by Wysoczańska et al. (2020b). They infer similar encounter parameters to the medians reported in Table 1, which is not surprising because Proxima Centauri's orbital period of 547^{+66}_{-40} kyr (Kervella et al. 2017) is much longer than the time to perihelion of 26.622 kyr (90% CI26.580–26.653 kyr).

5. Conclusions

This study has revealed 61 stars that, based on Gaia DR3 data, have passed—or will pass—within 1 pc of the Sun, most within ±6 Myr. Closer inspection reveals that 12 of these are probably not real encounters due to spurious measurements or being in close binaries. A further seven are in wide binaries, so their encounters are probably spurious unless their orbital periods are very long. As Gaia DR3 has much better precision and accuracy than previous Gaia releases, encounters within 1 pc identified using earlier Gaia releases that do not appear in Table 1 should generally be considered as obsolete. Potential exceptions are multiple systems in which the orbit of the center of mass has been traced, and stars with reliable non-Gaia astrometry.

In principle one could use these results to infer an overall stellar encounter rate, as was done in Bailer-Jones (2018) and Bailer-Jones et al. (2018b). Yet correcting for the significant

and poorly characterized incompleteness of the sample makes this difficult, and the result uncertain. This will be tackled using the larger sample expected in Gaia DR4. As close encounters generally have large ratios of radial velocities to transverse motions, contamination from spuriously large RVs is a problem. Resolved binaries not identified as such are also a source of contamination. But the individual encounters identified in this paper can be used to reassess Oort cloud comet perturbation or effects on specific comets (e.g., Dybczyński & Królikowska 2022).

To extend the identification of close encounters significantly beyond ±6 Myr we need to obtain RVs for fainter stars. There will be perhaps 100 million RVs in Gaia DR4 (Katz et al. 2022), and many will be near the faint limit of the RV survey, which is expected to extend two magnitudes deeper from the current limit of $G_{\rm RVS} = 14.0$ mag to $G_{\rm RVS} = 16.0$ mag (the bright limit in Gaia DR3 is $G_{\rm RVS} = 2.8$ mag). Although one can estimate an RV (or rather a probability distribution over the RV) for stars using their distances, transverse velocities, and a Galaxy model, and this will help to infer the statistics of encounters for fainter stars, this cannot be used to identify individual encounters reliably.

While we need more RVs, more precise proper motions will help to reduce the uncertainties on the encounter distances. This is because the closest encountering stars tend to have very low proper motions, and the lower the proper motion, the lower its uncertainty must be to retain a given S/N. Yet as proper motion precision improves as the $3/2$ power of the observation baseline duration, and Gaia DR3 is based on just under 3 yr of observations, we can expect significant improvements in Gaia DR4 (5 yr) and Gaia DR5 (expected to be 10.5–11 yr). The detection of astrometric orbits with Gaia will also help include or remove multiple stellar systems from the encounter lists.

I would like to thank Yves Frémat, Paola Sartoretti, and David Katz of the Gaia CU6 team, and Kareem El-Badry, for comments on the (un)reliability of white dwarf radial velocities. Thanks go also to the anonymous referee for useful suggestions. This work is based on data from the European Space Agency (ESA) mission Gaia (https://www.cosmos.esa.int/gaia), processed by the Gaia Data Processing and Analysis Consortium (DPAC, https://www.cosmos.esa.int/web/gaia/dpac/consortium). Funding for the DPAC has been provided by national institutions, in particular the institutions participating in the Gaia Multilateral Agreement. This research has made use of the Simbad object database (Wenger et al. 2000), the VizieR catalog access tool (Ochsenbein et al. 2000), and the Aladin sky atlas (Boch & Fernique 2014) (all operated at CDS Strasbourg: cds.u-strasbg.fr/), as well as NASAs Astrophysics Data System.

References

Andrae, R., Fouesneau, M., Sordo, R., et al. 2022, arXiv:2206.06138
Bagnulo, S., & Landstreet, J. D. 2020, A&A, 643, A134
Bailer-Jones, C. A. L. 2015a, A&A, 575, A35, Paper I
Bailer-Jones, C. A. L. 2015b, PASP, 127, 994
Bailer-Jones, C. A. L. 2018, A&A, 609, A8, Paper II
Bailer-Jones, C. A. L., Farnocchia, D., Meech, K. J., et al. 2018a, AJ, 156, 205
Bailer-Jones, C. A. L., Rybizki, J., Andrae, R., & Fouesneau, M. 2018b, A&A, 616, A37, Paper III
Bobylev, V. V., & Bajkova, A. T. 2017, AstL, 43, 559
Boch, T., & Fernique, P. 2014, in ASP Conf. Ser., 485, Astronomical Data Analysis Software and Systems XXIII, ed. N. Manset & P. Forshay (San Francisco, CA: ASP), 277
Brasser, R., Duncan, M. J., Levison, H. F., Schwamb, M. E., & Brown, M. E. 2012, Icar, 217, 1
Brown, G., & Rein, H. 2022, MNRAS, Advance Access
Dybczyński, P. A., Berski, F., Tokarek, J., et al. 2022, arXiv:2206.11047
Dybczyński, P. A., & Królikowska, M. 2022, A&A, 660, A100
El-Badry, K., Rix, H.-W., & Heintz, T. M. 2021, MNRAS, 506, 2269
Feng, F., & Bailer-Jones, C. A. L. 2015, MNRAS, 454, 3267
Finch, C. T., Zacharias, N., & Jao, W.-C. 2018, AJ, 155, 176
Gaia Collaboration, Smart, R. L., Sarro, L. M., et al. 2021, A&A, 649, A6
Gaia Collaboration, Vallenari, A., Brown, A. G. A., et al. 2022, A&A, in press
García-Sánchez, J., Weissman, P. R., Preston, R. A., et al. 2001, A&A, 379, 634
Gullberg, D., & Lindegren, L. 2002, A&A, 390, 383
Katz, D., Sartoretti, P., Guerrier, A., et al. 2022, arXiv:2206.05902
Kervella, P., Thévenin, F., & Lovis, C. 2017, A&A, 598, L7
Lindegren, L., Bastian, U., Biermann, M., et al. 2021a, A&A, 649, A4
Lindegren, L., Klioner, S. A., Hernández, J., et al. 2021b, A&A, 649, A2
Maíz Apellániz, J. 2022, A&A, 657, A130
Marigo, P., Girardi, L., Bressan, A., et al. 2017, ApJ, 835, 77
Ochsenbein, F., Bauer, P., & Marcout, J. 2000, A&AS, 143, 23
Ren, F., Chen, X., Zhang, H., et al. 2021, ApJL, 911, L20
Steinmetz, M., Matijevič, G., Enke, H., et al. 2020, AJ, 160, 82
Torres, S., Cai, M. X., Brown, A. G. A., & Portegies Zwart, S. 2019, A&A, 629, A139
Wenger, M., Ochsenbein, F., Egret, D., et al. 2000, A&AS, 143, 9
Wysoczańska, R., Dybczyński, P. A., & Królikowska, M. 2020a, MNRAS, 491, 2119
Wysoczańska, R., Dybczyński, P. A., & Polińska, M. 2020b, A&A, 640, A129
Zari, E., Hashemi, H., Brown, A. G. A., Jardine, K., & de Zeeuw, P. T. 2018, A&A, 620, A172
Zinn, J. C. 2021, AJ, 161, 214